Analysis of a filtered flamelet approach for coarse DNS of premixed turbulent combustion

S. Mukhopadhyay*, R.J.M. Bastiaans, J.A. van Oijen, L.P.H. de Goey

Combustion Technology , Department of Mechanical Engineering
Technische Universiteit Eindhoven
Den Dolech 2, 5600 MB Eindhoven, Netherlands

Abstract

Nowadays numerical simulations of premixed turbulent combustion can be performed at high spatial resolutions due to the continuously increasing computational power. At a resolution of the order of the laminar flame thickness there is negligible turbulence in the subgrid level and a proper reconstruction of the filtered flame is adequate for accurate predictions. This scenario, which can be termed as a coarse scale Direct Numerical Simulation (DNS), reconstruction of the filtered flame using a spatially filtered flamelet (1-D laminar flame) is analysed here. First, DNS of a turbulent premixed slot burner is computed to generate a reference database. This database is filtered at different length scales of the order of laminar flame thickness for an *a priori* assessment of turbulent flame reconstruction using a filtered flamelet. The filtered DNS source term, molecular diffusion and subgrid convection of the reaction progress variable is compared with a flamelet convoluted with top-hat profiles of the same order. The source term and molecular diffusion are approximated well from the filtered flamelet while the unresolved convection shows deviation. Finally, the reconstruction of the turbulent flame is tested *a posteriori* on the same filter widths (mesh size) and the results are compared. It is found that a flamelet filtered spatially at the order of the computational mesh and tabulated using a single controlling variable i.e. the reaction progress variable is suitable for a coarse scale DNS of premixed turbulent combustion.

Keywords: Turbulent premixed combustion, DNS, LES, Filtered Flamelet

*Corresponding author. Tel.: +31 40 247 3621.
Email address: sudiptomukhopadhyay@hotmail.com (S. Mukhopadhyay)

1. Introduction

Today a significant part of our energy needs is generated with devices burning hydrocarbon-air mixtures. Limited fuel resources as well as environmental concerns call for design of efficient combustion systems. In order to do so, numerical prediction of combustion has become an indispensable tool. Technical combustion devices rely on turbulence to enhance the power generation and their operation mostly takes place in the thin reaction zones (TRZ) regime [1]. Besides turbulence modeling, reduction of the combustion chemistry is a vital step, and along with the Reynolds number it determines the computational cost.

Reduction of chemistry by using tabulated chemistry methods like Flamelet Generated Manifolds (FGM) [2] or Flamelet Prolongation of Intrinsic Low Dimension Manifold (FPI) [3] enables prediction of intermediate species as well as pollutants [4]. This is achieved at much lower cost than using detailed mechanisms by decoupling chemistry from the flow and relaxing the resolution required for resolving the chemistry [5, 6]. A common approach is to treat the reacting flow with Computational Fluid Dynamics (CFD), to solve the Navier-Stokes equations supplemented by an equation for a progress variable (c). A (reaction) progress variable is a scalar that tracks the progress of the chemistry and is bound between the unburnt (0) to a completely burnt (1) state. Recently, a Hybrid Transported-Tabulated Chemistry (HTTC) approach [7] is introduced in which all the species which are non zero in fresh and burnt gases are transported with the flow and an optimized progress variable is defined from them. This ensures proper prediction of intermediates species which are expressed based on their self similar properties. In order to model adiabatic premixed combustion, a single controlling variable i.e. the progress variable is adequate if there is no significant differential diffusion [2]. A manifold constructed using FGM, in which the source term of the progress variable is a function of the progress variable, is an integral part of the system.

Let us consider what happens when performing a numerical simulation. On a computer we have to consider a discretized system and thus a certain continuous neighborhood should be contracted to a point. This discretization in space, gives rise to a filtered description of the system. To be consistent, we also have to filter

the manifold (in physical space). Now, if the size of the filter (Δ), which is implicitly applied to the system by the spatial discretization, tends to very small values, the system converges to DNS. For DNS of reacting flow, the filter size has to be small enough to resolve the reaction layer because in the TRZ regime of premixed turbulent combustion, the thickness of the reaction layer is smaller than the smallest fluid dynamic flow structures, defined by the Kolmogorov scale [1]. The latter scales can penetrate the preheat zone perturbing the flame structure but are too large to penetrate the reaction zone. Moreover, flow structures of the order of the Kolmogorov scale are only present in a temporal and spatial intermittent distribution (so not omnipresent). Therefore the strategy of using FGM for doing DNS of reacting flows in the TRZ regime is a good approximation as illustrated in e.g. [8].

As the mesh is coarsened and hence the filter size is increased, the flow will be gradually under-resolved starting with the reaction layer first. In particular, if the manifold would not be filtered, the source term would be misrepresented because there is insufficient resolution of the source term in physical space. If the filter size is of the order of the laminar flame thickness, there are negligible subgrid turbulent structures and the subgrid scale (SGS) variance then corresponds to the spatial resolution of the gradients produced by the reaction zone [9]. It is our assumption that in this scenario the subgrid scales can be determined from filtered flamelets. This assumption was verified in simulations of a turbulent Bunsen flame on a coarse grid with a mesh spacing of the order of the laminar flame thickness (δ_L) by Vreman et al. [10]. Here the term subgrid is used loosely to refer to phenomena that are unresolved, e.g., the reaction layer and does not necessarily mean that there are any turbulent structures at subgrid or subfilter level. Thus, by properly and consistently filtering the manifold we may be able to use relatively coarse grids to reduce the computational efforts.

With increasing filter size, filtered products of quantities start to deviate from products of these filtered quantities. Since only the filtered quantities are available, there is an additional closure problem that grows with filter size. This problem occurs mainly in two components of the transport equation of the progress variable: in the convective and in the diffusive terms. But here again, since we know the

laminar flame structure we also know the error associated and can correct for it. Fiorina et al. [11] considered this issue and demonstrated that by proper modeling it is possible to recover the laminar burning velocity for a 1-D laminar flame on a coarse computational grid.

If we go to larger filter sizes, i.e., $\Delta > \delta_L$ and of order Taylor microscale (λ), then we can find turbulent subgrid events and gradually enter the region of under-resolved hydrodynamic turbulence. In this case a subgrid model is required for the momentum equation and the flamelets become corrugated within the subgrid scales. Now, the information of the laminar flamelets becomes too limited and turbulent information should be taken into account. Modeling this is possible through a probability density function (PDF) of the occurrence of subgrid values of the progress variable source term. In principle this PDF would be a function of the moments of the local turbulence, typically mean and variance [12]. Often a presumed distribution like the β-function is used because of its ability to describe a multiple set of behaviors. This includes Gaussian like behavior but also, uni-modal, bi-modal and constant behavior. All these modes rely on the support of only two quantities, the mean and the variance.

It is the observation of the authors that there is a difference between coarse scale (or filtered) DNS and LES. Most literature on turbulent (premixed) combustion is not sensitive to this difference. The first regime can be considered as a coarse scale DNS (or Filtered Numerical Simulations) where stochastic events are almost negligible and modeling is limited to deterministic events which can be recovered from a filtered flame structure. The second regime can be considered as typical LES of reacting flows where the flame is completely subgrid and the stochastic events can exist in subgrid. Therefore, we divide the turbulent combustion modeling problem into two regimes:

- flame information that is not taken into account but can be reconstructed;
- turbulent flow information that is generally unknown and needs a statistical modeling approach.

It is interesting to investigate combustion modeling using laminar flame information, starting from the first regime (coarse DNS) and as the resolution is coarsened up

finally to the second regime (LES). Next, some available literature on the use of filtered laminar flame structure is discussed.

Filtered laminar flames have been investigated for modeling turbulent combustion by Boger et al. [13], Domingo et al. [14], Duwig [15], Vreman et al. [10], Fiorina et al. [11] and Moureau et al. [16]. Based on the filter size applied over the flame, these studies can be classified into two groups:

- flame filter size larger than computational mesh size [13, 14, 15, 11]
- flame filter size of the order of the computational mesh size [10, 16].

Some studies in the first group ([13, 14, 11]) use very large filter widths compared to the mesh size so that the filtered flame structure is resolved numerically by enough grid points in order to recover the correct laminar burning velocity like the Thickened Flame Model (TFM) [17]. However, in context of LES, the filtering operation is also applied to the velocity fields, unlike the thickening operation [15]. Further, the interaction of the filtered flame with subgrid turbulent structures is recovered through the use of a flame wrinkling factor or efficiency function. For example, a recent model F-TACLES [11] first attempts to recover the laminar flame speed (s_L^0) accurately and finally the turbulent burning velocity (s_T) is recovered by using a flame wrinkling factor. In F-TACLES the adequate resolution of the filtered laminar flame structure (i.e. over 5 grid points), is achieved by using very large filter widths. However, application of large filter width (e.g. 20 times δ_L [11]) changes the flame turbulence interaction from transport dominated to chemistry dominated regime. In addition, the flame wrinkling factor/efficiency function rather empirically modifies the source term and the molecular diffusion [1]. Duwig [15] performed successful LES of a dump combustor using a filter only 2 times the mesh/cell size to filter the flamelet and a small flame wrinkling factor.

In the second group of studies, the filter applied over the flamelet is of the order of the computational mesh size and the focus is on directly recovering the turbulent burning velocity. For example, Vreman et al. [10] used a flamelet spatially filtered with top-hat filter, of width equal to the computational mesh. The mesh size was of order of the laminar flame thickness, and resulted in good predictions for planar

Bunsen flames in the TRZ regime. Moureau et al. [16] proposed to close the filtered source term by convoluting the laminar flame with a filter smaller than the filter over the flow. This filtered laminar flame-PDF (FLF-PDF) method, was obtained through *a priori* analysis of DNS of a lean premixed swirl flame. FLF-PDF proposes to use two controlling variables, the mean and variance of progress variable, to take into account the effect of subgrid turbulence on chemistry like presumed PDF approaches. Notably, this study also demonstrated that the flame wrinkling factor fails in reproducing the correct subfilter PDF and thus questions simulations using this factor.

So far, turbulent combustion modeling using spatially filtered flamelets, is mostly focussed on using large filter widths compared to the mesh size in order to resolve the filtered structure [13, 14, 11] to recover the laminar flame speed (s_L^0) and finally the turbulent burning velocity (s_T) through flame wrinkling factor or efficiency function. However, it is also possible to model the chemical source term using flamelets filtered at the order of the mesh size [10, 16] by recovering correct turbulent burning velocity directly. In addition, the closure of filtered molecular diffusion and subgrid convection can also be achieved using the filtered flame structure [11]. Also most of the literature is devoted to combustion modeling in the scenario where there are turbulent structures in the subgrid and have to account their interaction with the flame. However, increasing computational power is offering spatial resolutions which preclude significant subgrid turbulence. In this scenario, it is interesting to investigate whether a flamelet filtered spatially at order of the mesh size can be used to close the various terms arising in the filtered progress variable transport equation and its accuracy.

In this work, we interrogate the region between DNS and LES, i.e., a regime of high-fidelity simulations which does not resolve the laminar flame structure but at the same time has negligible subgrid turbulence. This is done by looking at simulations with increasing filter size, from a resolution where the laminar flame is completely resolved (DNS) to where the flame is completely subgrid (a situation typical for LES of reacting flows). As a starting point, DNS of a premixed turbulent flame in the TRZ regime is performed using FGM. This is followed by an analysis of the filtered

DNS data to investigate the filter width, which applied over the 1-D laminar flame, can approximate the unresolved turbulent flame at mesh widths larger than DNS resolution. Based on the *a priori* analysis, it is found that by applying a filter width of the order of the computational mesh over the laminar flame solution, the filtered source term can be successfully closed on a mesh coarser than required for DNS as found earlier in [10, 16]. The closure of other terms in the filtered progress variable ($\tilde{c}$) equation , i.e., unresolved diffusion and convection of the progress variable as suggested in [11] is investigated for filter width of the order of the computational mesh size. Finally, the closure of the filtered progress variable equation using spatially filtered flamelet, namely, Filtered Flamelet Generated Manifold (FFGM) is tested *a posteriori* in the same configuration and the performance is compared with the DNS.

2. Direct numerical simulation of a turbulent slot flame

2.1. Governing equations

The governing equations that are solved under the low Mach assumption in reacting DNS, using a single controlling variable FGM are given below in vector notation:

$$\frac{\partial \rho}{\partial t} + \nabla \cdot (\rho \mathbf{u}) = 0, \tag{1}$$

$$\rho \left(\frac{\partial \mathbf{u}}{\partial t} + \mathbf{u} \cdot \nabla \mathbf{u} \right) = -\nabla p + \nabla \cdot (\mu \nabla \mathbf{u}) + \frac{\mu}{3} \nabla \left(\nabla \cdot \mathbf{u} \right), \tag{2}$$

$$\frac{\partial \rho c}{\partial t} + \nabla \cdot (\rho \mathbf{u} c) = \nabla \cdot (\rho D_c \nabla c) + \dot{\omega}_c, \tag{3}$$

where ρ, $\mathbf{u}$ and p represent density, velocity vector and pressure. The variables c, D_c and $\dot{\omega}_c$ denote progress variable, its mass diffusivity and its source term respectively. The diffusivity D_c in the premixed case is equal to D, the mixture averaged diffusivity divided by the Lewis number (Le) of the progress variable (c) chosen. In tabulated chemistry approach like FGM, $\rho = f_1(c)$, $\mu = f_2(c)$, $\dot{\omega}_c = f_3(c)$ and $D = f_4(c)$ are retrieved from a pre-computed table. Also other quantities like specific heat, temperature and species mass fractions are available as a function of the progress variable (c).

Commonly used numerics (including in this work), apply implicit filtering to the governing equations through the computational grid and discretization operators [18].

If a numerical grid is applied, values are ideally first filtered with a filter width that represents the physical spacing, which is equal to the grid size, and then sampled (at the grid points). This should be applied for the entire system including the manifold. So even in case of DNS, formally the equations (Eqs. 1-3) above should be overlined to show the filtering operation, how fine it may be but are avoided here for clarity. The solution converges towards DNS results as the grid is refined and not towards the solution of the filtered equations [18].

2.2. Numerical discretization

A low Mach number based finite volume solver [10, 19] written in Fortran 90 and parallelized using MPI and OpenMP standards is used to solve the above governing equations. For the continuity and momentum equations the standard finite volume method (FVM) is employed with second-order central differencing on a staggered Cartesian mesh. The scalar equation for transport of the progress variable is recast into the equivalent advective (non-conservative) formulation to which Van Leer's third-order accurate Monotone Upstream-centered Schemes for Conservation Laws (MUSCL) scheme, which is total variation diminishing (TVD), is applied.

For the temporal discretization, the explicit Euler method is used, except for the convective terms in the momentum equations, which are treated with second order Adams-Bashforth approach. The use of a first order temporal scheme for viscous fluxes is justified as small time steps are used (to maintain low CFL-number) and thus the spatial error dominates the temporal error [19]. After calculation of convective and viscous terms, the scalars and (uncorrected) velocities are updated to the new time level. Then the density, viscosity and source terms at the new time level are retrieved from the flamelet table using linear interpolation. Once the density at the new time level is known, the continuity equation provides the divergence of the momentum vector at the new time level. Applying the divergence operator to the momentum equation gives the Poisson equation for the pressure which is iteratively solved with a multigrid method.

2.3. Numerical setup

The computed flame configuration is a methane-air slot burner similar to earlier studies [20, 10, 19]. An unburnt CH_4 air mixture at stoichiometric condition issues

out from a slot of width, $w = 8$ mm with velocity, $U_{u0} = 3$ m/s and at $T_u = 300$ K ($c = 0$). A stoichiometric flame is chosen as it has the smallest laminar flame thickness. The unburnt jet is flanked on both sides by a co-flow with burnt products of the same composition issuing at $U_{b0} = 7$ m/s and $T_b = 2240$ K ($c = 1$). The expansion or heat release factor ($\tau = T_b/T_u - 1$) is around 6.5 and ratio of turbulent fluctuation to laminar flame speed (u'/s_L^0) is 2.4. The flame is considered periodic in spanwise direction. The mean inflow profiles for streamwise velocity and progress variable are prescribed as a tangent hyperbolic profile with a thickness based on the maximum derivative of c in the laminar flame solution. Turbulence at the inflow is generated by using a random number generator (URAND available with the Fortran90 compiler IFORT). These fluctuations are filtered spatially as well as temporally and then scaled to the desired turbulence level (further details are available in [10]). Perturbations are applied only to the unburnt mixture and the stencil used for generation of perturbations is the same for all simulations. A constant time step of $\Delta t = 1 \times 10^{-6} s$ is used to maintain a sufficiently low CFL number of 0.07 based on the velocity at inflow plane. This low CFL number also ensures that temporal error is insignificant compared to spatial discretization errors.

A freely propagating adiabatic laminar flame solution for stoichiometric methane air mixture at 300 K and standard atmospheric pressure is computed using GRI 3.0 mechanism [21] and the 1-D numerical flame solver CHEM1D [22]. The transport coefficients are computed with a mixture averaged model, i.e., Lewis numbers are non-unity. The normalised mass fraction of CO_2 was chosen as progress variable and the mass diffusivity D_c is computed by dividing the thermal diffusivity with its Lewis number (Le_{CO_2}). The chemistry (source term, mass fractions, temperature and other thermo-physical properties) was tabulated using 400 equidistant points in progress variable space to construct an FGM for the simulations.

2.4. DNS Results

Fig. 1 shows the wrinkled turbulent flame structure through an instantaneous 3-D snapshot of the iso-surface of $c = 0.55$ and the average flame shape through mean progress variable isocontours. The Taylor microscale and Kolmogorov scale along the centerline are plotted in Fig. 2.

DNS of turbulent combustion requires the flow scales as well as the chemical scales to be resolved. The estimated Kolmogorov scale, $\eta = (\nu^3/\epsilon)^{1/4}$, on the centerline at inflow plane is of the order of the DNS mesh size, $h = 0.1$ mm. The spatial resolution of $O(\eta)$ is generally adequate for DNS, as to obtain reliable first and second order statistics, the resolution should be fine enough to accurately capture most of the dissipation [23]. Here, most of the dissipation occurs at larger length scales near the flame front and thus the turbulence is adequately resolved. While using a progress variable formulation, the chemical scale is influenced by the choice of progress variable. The laminar flame thickness based on the maximum gradient of the progress variable (δ_c), is resolved with 5 points which is found to be sufficient (see e.g. [11]). The same spatial and temporal resolution has been used earlier for DNS of similar Bunsen flame with the same numerics in [24]. The parameters of the DNS are summarised in Table 1.

The stretch and curvature fields, obtained from the DNS computed with tabulated chemistry in this work, will differ from the one computed with detailed chemistry. However, they will not be much different as the differences introduced by FGM is approximately 5% [8].

3. Filtering the slot flame DNS

Affordable computations of realistic configurations often necessitate a mesh coarser than that required for a DNS, on which the chemistry (and flow) is not properly resolved. Finite Volume Method (FVM) based numerics, widely used in practical applications, impose an implicit filtering on the Navier-Stokes equations and scalar transport equation along with the spatial sampling. In case of a large filter (mesh) size a subgrid model is required to capture the effect of small flow scales and hence proper cascade of energy. In the TRZ regime with small (order of laminar flame thickness) filter (mesh) size, most of the flow structures are captured. However, chemical scales are still unresolved and necessitate a proper reconstruction.

In FGM-DNS the chemistry is coupled to the flow through progress variable (c) transport equation while on a grid coarser than DNS, a filtered equation is solved

for $\tilde{c}$. The exact filtered $\tilde{c}$ equation without any modeling reads as,

$$\frac{\partial \bar{\rho}\tilde{c}}{\partial t} + \nabla \cdot (\bar{\rho}\tilde{\mathbf{u}}\tilde{c}) = \nabla \cdot (\overline{\rho D \nabla c}) - \nabla \cdot (\bar{\rho}\widetilde{\mathbf{u}c} - \bar{\rho}\tilde{\mathbf{u}}\tilde{c}) + \bar{\dot{\omega}}_c \tag{4}$$

The filtered source term $\overline{\dot{\omega}}_c$, the filtered diffusion term $\nabla \cdot (\overline{\rho D \nabla c})$ and SGS flux of c given by $\nabla \cdot (\bar{\rho}\widetilde{\mathbf{u}c} - \bar{\rho}\tilde{\mathbf{u}}\tilde{c})$ require to be closed.

A common method of formulating closure models is through *a priori* analysis of DNS data by convoluting it with a filter in space. The spatial filtering enables to evaluate the terms appearing in the filtered progress variable equation for different filter widths and thus to evaluate the modeling approach. The filtering operation on a quantity ϕ can be denoted as

$$\overline{\rho\phi} = \bar{\rho}\tilde{\phi} = \int_{\mathcal{D}} \rho\phi G(\mathbf{x}, \xi) \mathrm{d}\xi, \tag{5}$$

where $\mathcal{D}$ is the flow domain. G is the filter kernel, here chosen as a top-hat defined by

$$\begin{aligned} G(\mathbf{x}, \xi) &= 1/\Delta^3 \quad \text{if} \quad |x_i - \xi_i| < \frac{1}{2}\Delta, \qquad i = 1, 2, 3, \\ &= 0, \qquad \text{otherwise} \end{aligned} \tag{6}$$

where Δ is the filter width applied to the DNS data.

An *a priori* analysis is carried out by filtering the DNS data at three different filter widths: 2 , 4 and 8 times h_{DNS} and then conditioned on $\tilde{c}$ before averaging in time. For the first two filter widths (2 and 4 times h_{DNS}), the laminar flame structure (based on gradient of progress variable) is resolved by approximately 3 and 2 points while for the largest filter width ($8h_{DNS}$) the laminar flame is entirely subgrid. The filter size of $8h_{DNS}$ corresponds to the Taylor microscale and is considered the ideal filter size for a well resolved LES. However, it is to be noted that the turbulence in the vicinity of the flame is damped due to the strong increase of kinematic viscosity (ν) with temperature. Thus, further downstream, the filter size of $8h_{DNS}$ is quite coarse in comparison to the integral scales existing in the vicinity of the flame front.

Fig. 3 shows the instantaneous source term and the same data filtered using the filter kernel G with $\Delta = 8h_{DNS}$ on the midplane $(y - z)$ of the slot burner. Further Fig. 4 shows scatter of the filtered source term in $\tilde{c}$ space for an instantaneous 3D field

corresponding to 18 flow through times. It can be seen that the scatter is very small in all the cases indicating a very limited presence of stochastic events in the subfilter space. However, with widening filter an increase in the scatter can be observed.

3.1. Filtered source term

We investigate here if a flamelet filtered in physical space (x) can model $\overline{\dot{\omega}}_c$ obtained from filtering the DNS of the turbulent flame computed in Section 2. Most 1-D flame solvers (like CHEM1D) compute the laminar flame solution in physical space. The distributions of various species as well as physical properties obtained in 1-D space are indicative of the spatial distribution in a real laminar flame. Spatial filtering of 1-D laminar flame solution is a quite straight forward operation. For sake of consistency with the filter applied to the DNS data, we choose a top-hat kernel to filter the 1-D flamelet. The top-hat kernel for filtering the 1-D flamelet is defined by

$$\begin{aligned} G_1(x,\xi) &= 1/\Delta_f \quad \text{if} \quad |x-\xi| < \frac{1}{2}\Delta_f, \\ &= 0 \qquad\quad \text{otherwise}, \end{aligned} \tag{7}$$

where Δ_f is the width of the filter with which the laminar flamelet is convoluted. The filtering of the chemical source term can then be represented simplified in one dimension as

$$\bar{\dot{\omega}}_c = \int_{-\infty}^{\infty} G_1(x,\xi)\dot{\omega}_c(c(\xi))\mathrm{d}\xi. \tag{8}$$

The effect of filtering a 1-D laminar flame in physical space at widths 2, 4 and 8 times of DNS mesh size is shown in Fig. 5. When looking at a global level it is clear that these small filters have a marginal effect on the filtered progress variable. However, on a smaller scale and in particular if the source term is considered, than we see much larger differences. Furthermore it can be observed (especially from the zoom of the source term) that a mesh size of 0.1 mm in the DNS is at the edge of being sufficient to capture the source term. The same filtered source terms when transformed to progress variable space are shown in Fig. 6. The filtered, conditioned and time averaged source term from the DNS for comparison with the filtered laminar source term is also shown in Fig. 6. For time averaging, DNS fields are accumulated after two flow through times have elapsed and in total 50 fields distributed over 18 flow through times are used.

3.2. Flame filter size

The question that now arises is: what should be the width of the filter to be used for filtering the 1-D laminar flame solution? For the choice of filter width over the laminar flame, Δ_f, an obvious choice will be the filter width Δ, at which the DNS results are filtered as in [10]. From Fig. 6, it turns out that this choice produces a reasonable approximation to the source term from filtered DNS. However, $\Delta_f < \Delta$ was found in [16]. So we filter the laminar flamelet at different widths, to find a filter width which yields best fit with each Δ filtered 3-D DNS source term. By comparing visually and the integrated area under the curves, an optimum filter width over the flame i.e. $\Delta_f = \Delta_f^o$ is determined for all three cases and the filtered 1-D source terms are shown in Fig. 7.

The filtered source term $\bar{\dot{\omega}}_c$ from the DNS filtered at Δ and 1-D flamelet filtered at Δ_f^o for all cases is presented in Fig. 7. Good agreement is observed for the smaller Δ = 2 and 4 times h_{DNS}, while for the largest filter width, $\Delta = 8h_{DNS}$ agreement is not as good. The results for optimal filter width (Δ_f^o) show that the flame filtered at a suitable width can capture the source term distribution at a coarse filter ($\Delta > h_{DNS}$). The filter widths used for filtering the DNS field and the corresponding filter widths applied to 1-D flame solutions to achieve the same level of filtered source term are summarised in Table 2. The trend that emerges from the *a priori* analysis, is that Δ_f^o and Δ are of same order with the ratio Δ_f^o/Δ being slightly greater than 1. The findings are somewhat different to that of the FLF-PDF model [16], which finds Δ_f^o/Δ being less than 1. Though there is a difference in the Δ_f^o/Δ ratio, the widths are found to be of the same order in both the studies.

The small difference can be attributed to various factors. First, a stoichiometric mixture is used in our study, which has a higher heat release rate than the lean mixture (equivalence ratio 0.7) used in [16]. Second, a top-hat kernel was used in this work whereas a Gaussian kernel was used in [16]. While the shape of the kernel does not affect the averaged filtered DNS output, it does impact the convoluted 1-D laminar flame. Filtered laminar source terms for a Gaussian and top-hat kernel of equal widths are shown in Fig. 8 and indicate different distributions for the larger filter widths. The extent of turbulence in the present case (Re_λ=60) is different

from the other case (Re_λ=150) and thus the turbulent burning velocity is impacted. Third, we chose the normalised mass fraction of CO_2 as progress variable while in [16] a combination of CO_2 and CO was used. The choice of progress variable alters the distribution of $\dot{\omega}_c$ in physical as well as c space. Also the flame resolution and dynamics are affected through the gradient of c. Lastly, there is a difference in spatial discretization which is 2nd order in present study and 4th order in the other case.

The filtered source term closure in [16] also depends on a second controlling variable, namely, the variance of c, defined as $c_v = \widetilde{cc} - \tilde{c}\tilde{c}$. The variance of c, computed from the Δ filtered DNS field (conditioned and time averaged) and the Δ_f^o filtered laminar flame is presented in Fig. 9. Perfect agreement for c_v from the filtered DNS and filtered flamelet is found at smallest filter width, i.e., 2 times h_{DNS} proving the assumption made earlier that a spatially filtered flamelet can be used to reconstruct the unresolved flame. Thus at small filter size a single controlling variable, $\tilde{c}$ is adequate for accurate resolution of chemistry and we use the same here in this work. The agreement of c_v in the preheat zone decreases with increasing filter width but the agreement remains quite good on the burnt side. Discrepancies at the unburnt side ($c < 0.5$) can be attributed to SGS structures present in the unburnt mixture as reported earlier in [16].

3.3. Unresolved Molecular Diffusion

As mentioned earlier, with increasing filter size the filtered product of quantities deviate more from the product of filtered quantities. This effect in the modeling of the diffusion term is investigated here. In the filtered progress variable ($\tilde{c}$) equation, the molecular diffusion term is often approximated in the numerical simulations as

$$\nabla \cdot (\overline{\rho D \nabla c}) \approx \nabla \cdot (\overline{\rho D} \nabla \tilde{c}). \tag{9}$$

A more accurate representation (exact in 1-D) of this term follows from [11] as

$$\nabla \cdot (\overline{\rho D \nabla c}) = \nabla \cdot (\alpha_c \overline{\rho D} \nabla \tilde{c}), \tag{10}$$

where the correction factor defined as

$$\alpha_c(\tilde{c}) = \frac{\overline{\rho D |\frac{\partial c}{\partial x}|}}{\overline{\rho D} |\frac{\partial \tilde{c}}{\partial x}|}, \tag{11}$$

is computed from the 1-D filtered flame and is tabulated as a function of $\tilde{c}$. $\alpha_c(\tilde{c})$ is also computed using the filtered DNS data along the streamwise direction (z). In Fig. 10, α_c computed from the DNS filtered at Δ and from the 1-D flame filtered at corresponding Δ_f^o are plotted and shows good agreement. This figure also shows that the values of α_c increase with increasing filter width and are higher in the cold regions of the flame (c close to 0) for a given filter width. Traditional modeling approach like Eq. (9) leads to $\alpha_c = 1$. The unresolved diffusion is well modeled with this formulation even though the flame is strongly curved with a radius in the order of the flame thickness.

One of the main advantages of flamelet methods like FGM is that in the colder zone of the flame the molecular diffusion process which affects the chemical balance between chemical production and consumption is captured correctly [2]. Including α_c will improve the numerical modeling of the diffusion term (in comparison to Eq. (9)), leading to accurate molecular diffusion in the preheat zone of the flame.

3.4. Unresolved scalar transport

Filtering of the progress variable equation gives rise to an unclosed convective term commonly represented as $-\nabla \cdot (\bar{\rho}\widetilde{\mathbf{u}c} - \bar{\rho}\tilde{\mathbf{u}}\tilde{c})$. This unresolved (or subgrid) convection and the resolved part, $\nabla \cdot (\bar{\rho}\tilde{\mathbf{u}}\tilde{c})$, is computed from the DNS database for different filter widths. The unresolved convection becomes significant in comparison to the resolved transport of $\tilde{c}$ with increasing filter size [25].

Fig. 11 shows the streamwise direction (the predominant flow direction), SGS transport, $\bar{\rho}(\widetilde{wc} - \tilde{w}\tilde{c})$, obtained from filtering the DNS field and the conditioned gradient of $\tilde{c}$. Both quantities are positive for all the filter widths and thus indicate counter-gradient diffusion (CGD). The counter-gradient diffusion in this case can be explained on the basis of high heat release rate and low ratio of turbulence intensity to laminar flame speed [26]. In case of a high heat release factor, CGD is promoted and it is observed in some studies even at high turbulence intensity.

The filtering operation induces unresolved scalar fluxes even in a laminar 1-D flame [25, p. 270]:

$$\bar{\rho}(\widetilde{uc} - \tilde{u}\tilde{c}) = \rho_0 s_L^0(\bar{c} - \tilde{c}), \tag{12}$$

where the laminar flame speed (s_L^0) and the unburnt gas mixture density (ρ_0) are

available from 1-D flame computations. It is to be noted here that Eq. (12) is exact for a 1-D laminar flame. The divergence of Eq. (12) arising from the 1-D filtered laminar flame can be incorporated as [11],

$$\Omega_c = -\rho_0 s_L^0 \left(\frac{\partial \bar{c}}{\partial x} - \frac{\partial \tilde{c}}{\partial x} \right), \tag{13}$$

where the gradients are computed from the laminar flamelet filtered in physical space. Following [25, 11], the total unresolved scalar flux is closed as

$$-\nabla \cdot (\widetilde{\bar{\rho}\mathbf{u}c} - \bar{\rho}\tilde{\mathbf{u}}\tilde{c}) = \Omega_c. \tag{14}$$

Fig. 12 shows the unresolved convective flux computed from the 1-D filtered laminar flame (Ω_c) and from the filtered DNS (-$\nabla \cdot (\widetilde{\bar{\rho}\mathbf{u}c} - \bar{\rho}\tilde{\mathbf{u}}\tilde{c})$) for filter widths $\Delta = 2, 4$ and 8 h_{DNS}. In this work, we find that Ω_c increasingly deviates from $-\nabla \cdot (\widetilde{\bar{\rho}\mathbf{u}c} - \bar{\rho}\tilde{\mathbf{u}}\tilde{c})$ with increase in filter size. The deviation is very small in case of $\Delta = 2h_{DNS}$ but significant in $\Delta = 8h_{DNS}$. It is to be noted here that although the term Ω_c represents the unresolved or SGS convection of $\tilde{c}$ exactly in 1-D, it does not in 3-D. Also, it assumes that the mass burning rate is that of an unstretched flame, an assumption not necessarily true in 3D turbulent flows. However, the trend (CGD) is captured qualitatively and further improvement in modeling of SGS convection of progress variable is not attempted at this stage.

4. Filtered Flamelet Generated Manifold

The filtered equation for progress variable Eq. (4) can be closed using the closure models described previously in Eq. (10) and Eq. (14) along with the source term from a spatially filtered manifold and reads as follows:

$$\frac{\partial \bar{\rho}\tilde{c}}{\partial t} + \nabla \cdot (\bar{\rho}\tilde{\mathbf{u}}\tilde{c}) = \nabla \cdot \left(\alpha_c \overline{\rho D} \nabla \tilde{c} \right) + \Omega_c + \bar{\dot{\omega}}_c. \tag{15}$$

It is to be noted here that in [10] the source term was closed by filtering a laminar flame with filter size of the mesh but the terms diffusion correction factor (α_c) and subgrid convection (Ω_c) as proposed in [11] were not used. However, [11] uses large filter width (compared to mesh width) to spread the filtered flame structure over a number of grid points and the flame wrinkling factor to recover turbulent burning

velocity (as in thickened flame method). From *a priori* analysis in [16], it was proposed that the filtered source term can be recovered using flamelet filtered at size smaller than the mesh size but the modeling of other terms were not discussed.

In this work, we attempt to close the transport equation of $\tilde{c}$, Eq. (4) , by using a flamelet filtered at the order of the mesh size to obtain the filtered source term ($\bar{\dot{\omega}}_c$) as in [10, 16], diffusion correction factor (α_c) and subgrid convection (Ω_c)as in [11]. The present formulation does not require any flame wrinkling factor unlike [11]. For sake of convenience, we refer the formulation in Eq. (15) as Filtered Flamelet Generated manifold (FFGM) and is implemented in the code described earlier. In the next section, we investigate the performance of FFGM *a posteriori*.

4.1. A posteriori analysis

The same slot flame configuration is tested using the FFGM approach. The terms α_c, Ω_c and the filtered source term $\overline{\dot{\omega}}_c$ are computed from the 1-D filtered laminar flame and tabulated as a function of $\tilde{c}$, for the flame filter size Δ_f^o. Assuming that the filter size is equal to the mesh size, three *a posteriori* simulations are carried out with grid spacing, h_x = 2, 4 and 8 times h_{DNS} to benchmark against DNS data. For each of the simulations, the manifold is constructed using a 1-D laminar flame filtered with a top-hat at corresponding Δ_f^o obtained from the *a priori* analysis and then tabulated as a function of $\tilde{c}$.

To give an impression of the FFGM results compared to the DNS results we repeat the results of Figs. 1 and 3 for direct comparison with Figs. 13 and 14. It is clear that the FFGM results deteriorate from the DNS at coarser grids. The finest FFGM looks very much like the DNS result of Fig. 3. The wrinkling looks similar and one can even see an unburnt pocket in both cases. If one looks at the coarser FFGM's the agreement is becoming less convincing. However, one has to take into account that one has to compare the filtered version in Fig. 3 with the coarsest version in Fig. 14. If we consider these results in this framework, we can conclude that the deterioration is acceptable.

The average flame shape, an important characteristic of a Bunsen flame, is chosen to benchmark FFGM. The flame shape is computed based on isocontour of $c = 0.55$ (corresponding to maximum source term) averaged in periodic direction and in time.

The simplest model for the filtered source term is the trivial model or zero model, simply denoted as $\bar{\dot{\omega}}_c = \dot{\omega}_c(\tilde{c})$. The zero model is implemented by using an unfiltered manifold along with setting $\alpha_c = 1$ and $\Omega_c = 0$ in Eq. (15). The comparison carried out against the zero model (unfiltered) case and DNS prediction is shown in Fig. 15. It shows that for 2 times h_{DNS} the FFGM and zero model both predict a slightly taller flame with FFGM slightly better than the zero model. In case of the intermediate mesh size, i.e., 4 times h_{DNS}, the FFGM prediction is very close to DNS and better than that from the zero model. However, the effect of FFGM is strongly noticeable in the case of the coarsest grid, $h_x = 8h_{DNS}$ where it clearly shows that the FFGM is better than the zero model. It is to be mentioned here that FFGM constructed using a Gaussian kernel performs almost similar.

Fig. 16 shows the mean values of the progress variable and its source term at the centerline along the stream wise direction predicted by FFGM for different filter widths. The prediction of $\tilde{c}$ exhibits the same trend as observed in case of the flame height. The source term distribution along the centerline can be correlated with the flame height as a higher source term indicates faster burn out, leading to a shorter flame. The variances are relevant but not shown as DNS should be filtered to compare fluctuating quantities or a subgrid model is required to retrieve the SGS part of the fluctuations [10].

It is interesting to investigate the effects of different closures in the filtered progress variable transport equation. The various terms can be investigated by setting them to values without including components from filtered laminar flame. The effect of the diffusion correction can be omitted by setting $\alpha_c = 1$ and the subgrid convection can be omitted by setting $\Omega_c = 0$ in Eq. (15). Fig. 17 shows the effect of the different closure terms through the flame shape represented by $\tilde{c} = 0.55$. It can be seen that in case of small filter width $2h_{DNS}$ the closure terms do not play a significant role and molecular diffusion (α_c) is as important as SGS convection (Ω_c). However, at large filter width, i.e., $8h_{DNS}$ the terms are significant with Ω_c being more significant than α_c.

4.2. Computational cost

With the flamelet approach the reduction in simulation time is already significant [4] and gains achieved with FFGM model are presented here. The FFGM model is able to predict the flame shape quite well for the fine mesh, e.g., 2 and 4 times h_{DNS}. For a coarse grid in which the flame is completely subgrid, the results are not satisfactory, for which the reasons are explained in the next section. It is interesting to compare the computational gains and the error associated with it. An error estimate can be computed based on the maximum flame height (based on isocontour $c = 0.55$) predicted by various simulations with respect to that predicted by DNS. The error is defined as the difference in mean flame height at the centerline with respect to the one computed in DNS. The table showing computational gains along with the associated error is summarised in Table 3. It is evident that FFGM predicts combustion quite reasonably on fine meshes and is computationally much cheaper than DNS.

4.3. Analysis of FFGM results

Prediction using FFGM reconstruction is good for the smaller mesh sizes while it tends to go off the mark with large mesh size. The degeneration in the performance of the model with increasing filter width or grid size can be attributed to various factors.

In *a posteriori* simulations it is assumed that the filter width is equal to the mesh size, $\Delta = h_x$ (a prevalent approach in implicit LES) but this is often not true. It is difficult to determine the effective filter size in implicit simulations and hence the assumed filter width $\Delta = h_x$ may be inaccurate [27]. Also, numerical diffusion can alter the effective filter on the flame. Numerical diffusion of progress variable is needed to keep the scalars between their physical bounds. Because of the change in the effective Δ it is expected that the actual Δ_f will differ from the one found *a priori* from DNS. Also, at a filter size equal to the mesh size the solution embodies the highest error. For the numerics used here, the discretization error involved with spatial derivatives in convective and viscous term turns out to be relatively large compared to subgrid part [10] which implies that the observed differences were most probably influenced by discretization error. In *a posteriori* simulations the actual

coarsening of the grid causes a resampling of the data additional to the filtering effect. At a very coarse mesh size it is possible that the discretization error overwhelms the model performance. Thus, it is possible that a particular value of Δ_f other than Δ_f^o is more effective in *a posteriori* simulations.

To investigate this possibility, a couple of *a posteriori* simulations have been performed with different Δ_f values in the vicinity of Δ for mesh sizes of $h_x = 4h_{DNS}$ and $h_x = 8h_{DNS}$, which are significantly cheaper to compute. A filter width $\Delta_f = \Delta_f^x$ could be found which produced the flame shape based on $\tilde{c} = 0.55$ better than one using $\Delta_f = \Delta_f^o$ (filter width from *a priori* DNS). For $h_x = 4h_{DNS}$, a filter $\Delta_f^x = 3h_{DNS}$ and for $h_x = 8h_{DNS}$, a filter $\Delta_f^x = 12h_{DNS}$ are appropriate respectively. Fig. 18 shows the flame shape based on $\tilde{c} = 0.55$ for $\Delta_f = \Delta, \Delta_f^o$ and Δ_f^x . It can be seen that the flame shape differs very little for flames filtered with Δ and Δ_f^o. So in real life simulations where Δ_f can not be computed beforehand because DNS data is not available, filtering the manifold at mesh size Δ is practical and a good choice. In Fig. 19 the overall flame structure represented by isocontours of c for $h_x = 4h_{DNS}$ and $h_x = 8h_{DNS}$ for flamelet filtered at Δ_f^x is plotted and can be compared with the DNS flame structure represented by average isocontours of c in Fig. 1. The flame structures compare well, with a slight reduction in flame spread as compared to DNS, which is expected due to loss of fluctuations on a coarse grid and filtering of the flame. At these iterative filter widths probably the modeling and discretization errors cancel out, yielding a correct flame shape. These iterative simulations are not feasible in realistic computations and are just used to illustrate the potential of the method when an optimal Δ_f is used (*a posteriori*).

Looking at the unresolved convection *a priori*, one can conclude that modeling this term with Ω_c from a filtered laminar flame is not a good approximation at larger filter widths. Also, the *a priori* filtered source term deviates at large filter widths in the preheat zone. The error in the filtered source term modeling using FFGM normalised by a quantity independent of the filtering can be computed as

$$\epsilon_{\bar{\dot{\omega}}_c} = \left[\frac{(\bar{\dot{\omega}}_c^{FFGM} - \bar{\dot{\omega}}_c^{DNS})^2}{(\dot{\omega}_c^{DNS})^2} \right]^{1/2} .$$

Fig. 20 shows semilog plot of $\epsilon_{\bar{\dot{\omega}}_c}$ conditioned on $\tilde{c}$ and time averaged. Significant deviations can be seen at the unburnt side due to inadequate closure of the source

term by a flamelet filtered at a single scale. It is to be noted that the coarsest mesh used here is larger than the laminar flame thickness.

5. Conclusions

In this work, a filtered flamelet approach is analysed to investigate the modeling of premixed turbulent combustion at spatial resolutions of the order of the laminar flame thickness. In this scenario, most of the turbulence is resolved and there is very little statistics left in the subgrid. Based on *a priori* analysis of DNS data, it was found that the source term and the filtered molecular diffusion can be closed accurately by filtering a 1-D laminar flame solution with top-hat filter having width of the order of the computational mesh. However, the closure of the unresolved convection of progress variable was found to exhibit deviations that increase with the filter size. This approach, namely, Filtered Flamelet Generated Manifold (FFGM) was tested *a posteriori* and compared with the DNS results. Comparisons show good agreement for mesh sizes smaller than the laminar thickness whereas for situations where the flame is completely subgrid the agreement decreases. Thus, a laminar flame solution spatially filtered at the mesh size, can be used for a coarse scale DNS of premixed turbulent flame, with a satisfactory performance. The filtering applied to the velocity fields and the manifold are of the same order in this approach. The reduction in spatial resolution achieved by a coarse DNS yields significant reduction in computational effort and thus can be used as a benchmark for coarser simulations i.e. LES. Further investigations are required for the subgrid convection closure, *a posteriori* performance in highly turbulent flows and the effective filter imposed in filtered simulations.

Acknowledgements

Support from Dutch Technology Foundation (STW) and Rolls-Royce is gratefully acknowledged. The authors would also like to express their gratitude to Dr. A.W. Vreman for many useful discussions.

References

[1] Pitsch H. Large-Eddy Simulation of Turbulent Combustion. Annual Review of Fluid Mechanics 2006;38:453–82.

[2] van Oijen JA, de Goey LPH. Modelling of premixed laminar flames using flamelet-generated manifolds. Combustion Science and Technology 2000;161:113–37.

[3] Gicquel O, Darabiha N, Thévenin D. Laminar premixed hydrogen/air counterflow flame simulations using flame prolongation of ILDM with differential diffusion. Proceedings of the Combustion Institute 2000;28:1901 –8.

[4] Ren Z, Yang H, Lu T. Effects of small-scale turbulence on NOx formation in premixed flame fronts. Fuel 2014;115:241 –7.

[5] Olbricht C, Stein OT, Janicka J, van Oijen JA, Wysocki S, Kempf AM. LES of lifted flames in a gas turbine model combustor using top-hat filtered PFGM chemistry. Fuel 2012;:1–8.

[6] Egüz U, Leermakers N, Somers B, de Goey P. Modeling of PCCI combustion with FGM tabulated chemistry. Fuel 2014;118:91 –9.

[7] Ribert G, Vervisch L, Domingo P, Niu YS. Hybrid transported-tabulated strategy to downsize detailed chemistry for numerical simulation of premixed flames. Flow, Turbulence and Combustion 2014;92:175–200.

[8] van Oijen JA, Bastiaans RJM, de Goey LPH. Low-dimensional manifolds in direct numerical simulations of premixed turbulent flames. Proceedings of the Combustion Institute 2007;31:1377 –84.

[9] Domingo P, Vervisch L, Payet S, Hauguel R. DNS of a premixed turbulent V flame and LES of a ducted flame using a FSD-PDF subgrid scale closure with FPI-tabulated chemistry. Combustion and Flame 2005;143:566 –86.

[10] Vreman AW, van Oijen JA, de Goey LPH, Bastiaans RJM. Subgrid Scale Modeling in Large-Eddy Simulation of Turbulent CombustionUsing Premixed Flamelet Chemistry. Flow, Turbulence and Combustion 2008;82:511–35.

[11] Fiorina B, Vicquelin R, Auzillon P, Darabiha N, Gicquel O, Veynante D. A filtered tabulated chemistry model for LES of premixed combustion. Combustion and Flame 2010;157:465 –75.

[12] Guo Z, Zhang H, Chan C, Lin W. Presumed joint probability density function model for turbulent combustion. Fuel 2003;82:1091 –101.

[13] Boger M, Veynante D, Boughanem H, Trouvé A. Direct numerical simulation analysis of flame surface density concept for large eddy simulation of turbulent premixed combustion. Proceedings of Combustion Institute 1998;27:917 –25.

[14] Domingo P, Vervisch L, Bray K. Partially premixed flamelets in LES of non-premixed turbulent combustion. Combustion Theory and Modelling 2002;6:529–51.

[15] Duwig C. Study of a Filtered Flamelet Formulation for Large Eddy Simulation of Premixed Turbulent Flames. Flow, Turbulence and Combustion 2007;79:433–54.

[16] Moureau V, Domingo P, Vervisch L. From Large-Eddy Simulation to Direct Numerical Simulation of a lean premixed swirl flame: Filtered laminar flame-PDF modeling. Combustion and Flame 2011;158:1340–57.

[17] Colin O, Ducros F, Veynante D. A thickened flame model for large eddy simulations of turbulent premixed combustion. Physics of Fluids 2000;12:1843–63.

[18] Janicka J, Sadiki A. Large eddy simulation of turbulent combustion systems. Proceedings of the Combustion Institute 2005;30:537–47.

[19] Ramaekers WJ, van Oijen JA, de Goey LPH. Stratified turbulent Bunsen flames: flame surface analysis and flame surface density modelling. Combustion Theory and Modelling 2012;16:943–75.

[20] Bell JB, Day MS, Grcar JF, Lijewski MJ, Driscoll JF, Filatyev SA. Numerical simulation of a laboratory-scale turbulent slot flame. Proceedings of the Combustion Institute 2007;31:1299–307.

[21] Smith GP, Golden DM, Frenklach M, Eiteener B, Goldenberg M, Bowman CT, et al. GRI-Mech 3.0. http://www.me.berkeley.edu/gri-mech/; 2000.

[22] Somers LMT. The simulation of flat flames with detailed and reduced chemical models. Ph.D. thesis; Technische Universiteit Eindhoven; 1994.

[23] Moin P, Mahesh K. Direct Numerical Simulation: A Tool in Turbulence Research. Annual Review of Fluid Mechanics 1998;30:539–78.

[24] Vreman AW, Bastiaans RJM, Geurts BJ. A Similarity Subgrid Model for Premixed Turbulent Combustion. Flow, Turbulence and Combustion 2008;82:233–48.

[25] Poinsot T, Veynante D. Theoretical And Numerical Combustion; T. Poinsot; third ed.; 2012.

[26] Veynante D, Trouvé A. Gradient and counter-gradient scalar transport in turbulent premixed flames. Journal of Fluid Mechanics 1997;332:263–93.

[27] Rogallo RS, Moin P. Numerical simulation of turbulent flows. Annual Review of Fluid Mechanics 1984;:99–137.

Tables

Table 1: DNS parameters of the slot burner

Parameter	Value
laminar flame thickness (δ_L)	0.512 mm
DNS mesh spacing (h_{DNS})	0.1 mm
Fuel composition	stoichiometric CH_4-air
Temperature of unburnt mixture (T_u)	300 K
Pressure (p)	1 bar
Heat release factor (τ)	6.5
slot width (w)	8 mm
Reynolds number based on Taylor microscale (Re_λ)	60
rms velocity at inflow/laminar flame speed (u'/s_L^0)	2.4
Kolmogorov scale at centerline on inlet (η)	0.06 mm
Minimum Taylor microscale at centerline (λ)	0.82 mm
Karlovitz number at centerline for $\langle c \rangle = 0.05$ (Ka)	18

Table 2: Filter widths over DNS and Flame

Δ/h	Δ_f^o/h	δ_L/Δ
2	2.5	2.6
4	4.5	1.3
8	9.0	0.6

Table 3: Computational cost of turbulent Bunsen flame simulations

Simulation	h_x [mm]	Mesh	δt [10^{-5} s]	CPU time [hours]	Error [%]
DNS	0.1	$160 \times 256 \times 320$	0.1	5984	-
FFGM	0.2	$80 \times 128 \times 160$	0.5	560	7.8
FFGM	0.4	$40 \times 64 \times 80$	1.0	72	-4.16
FFGM	0.8	$20 \times 32 \times 40$	1.0	10	-12.31

Figures

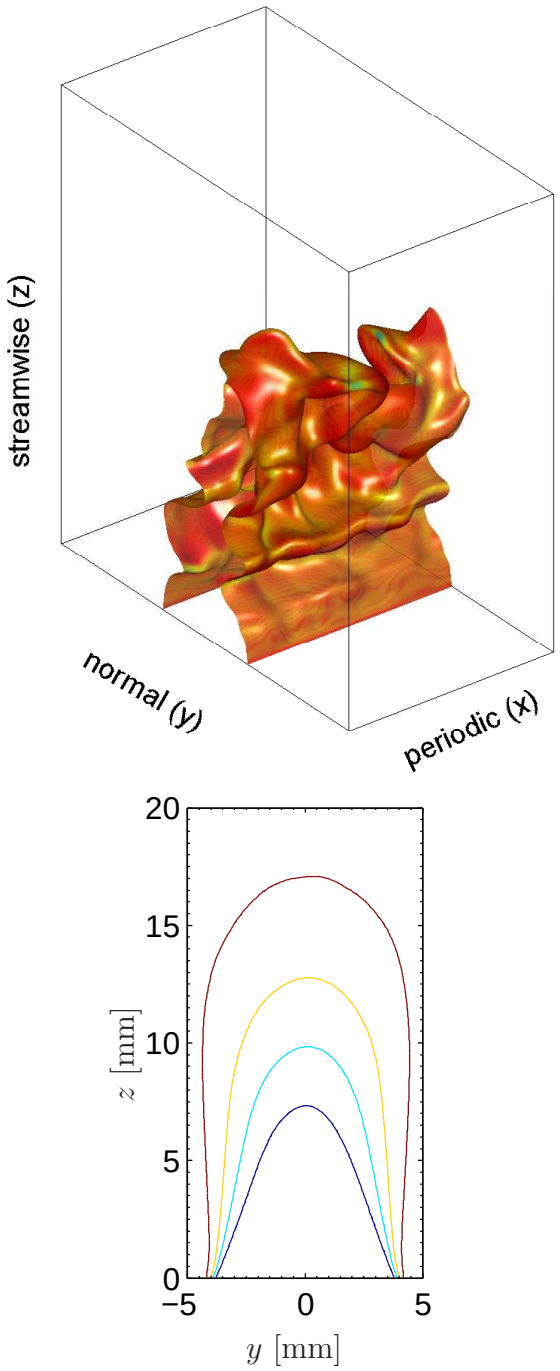

Figure 1: Turbulent Bunsen flame Top: Instantaneous snapshot of progress variable isocontour c = 0.55. The color represents the gradient of c. Bottom: Time averaged isocontours of c = 0.2, 0.4, 0.6 and 0.8.

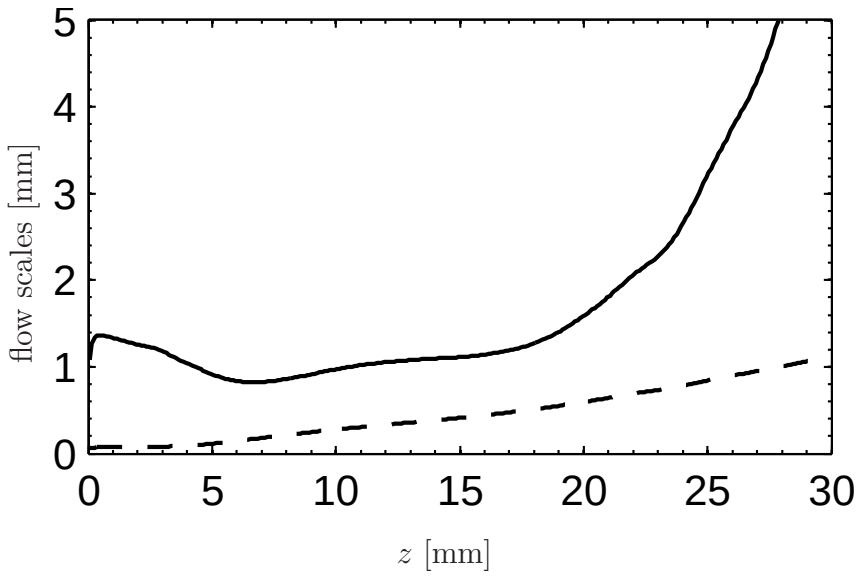

Figure 2: Streamwise flow conditions computed at the centerline in the DNS. Top: Mean (solid) and RMS (dashed) velocities. Bottom: Taylor microscale (solid) and Kolmogorov scale (dashed).

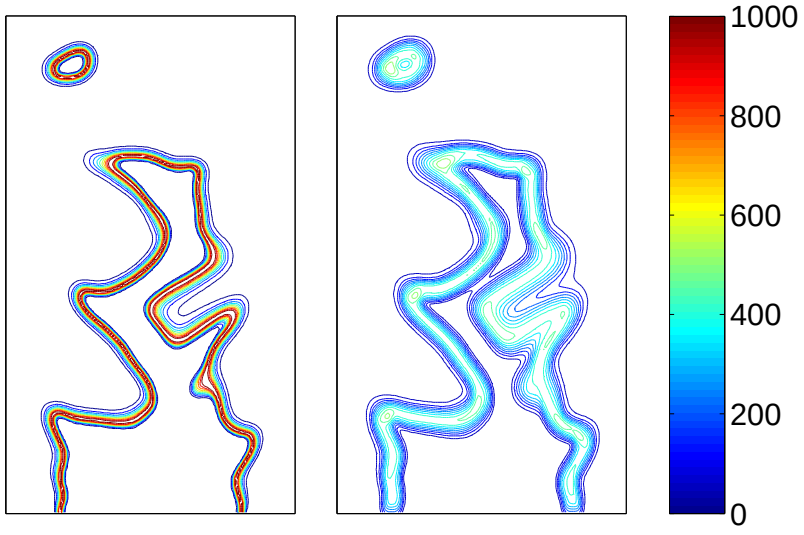

Figure 3: Instantaneous source term $\dot{\omega}_c$ $[kg/m^3s]$ - DNS (left) and spatially filtered DNS with $8h_{DNS}$ (right).

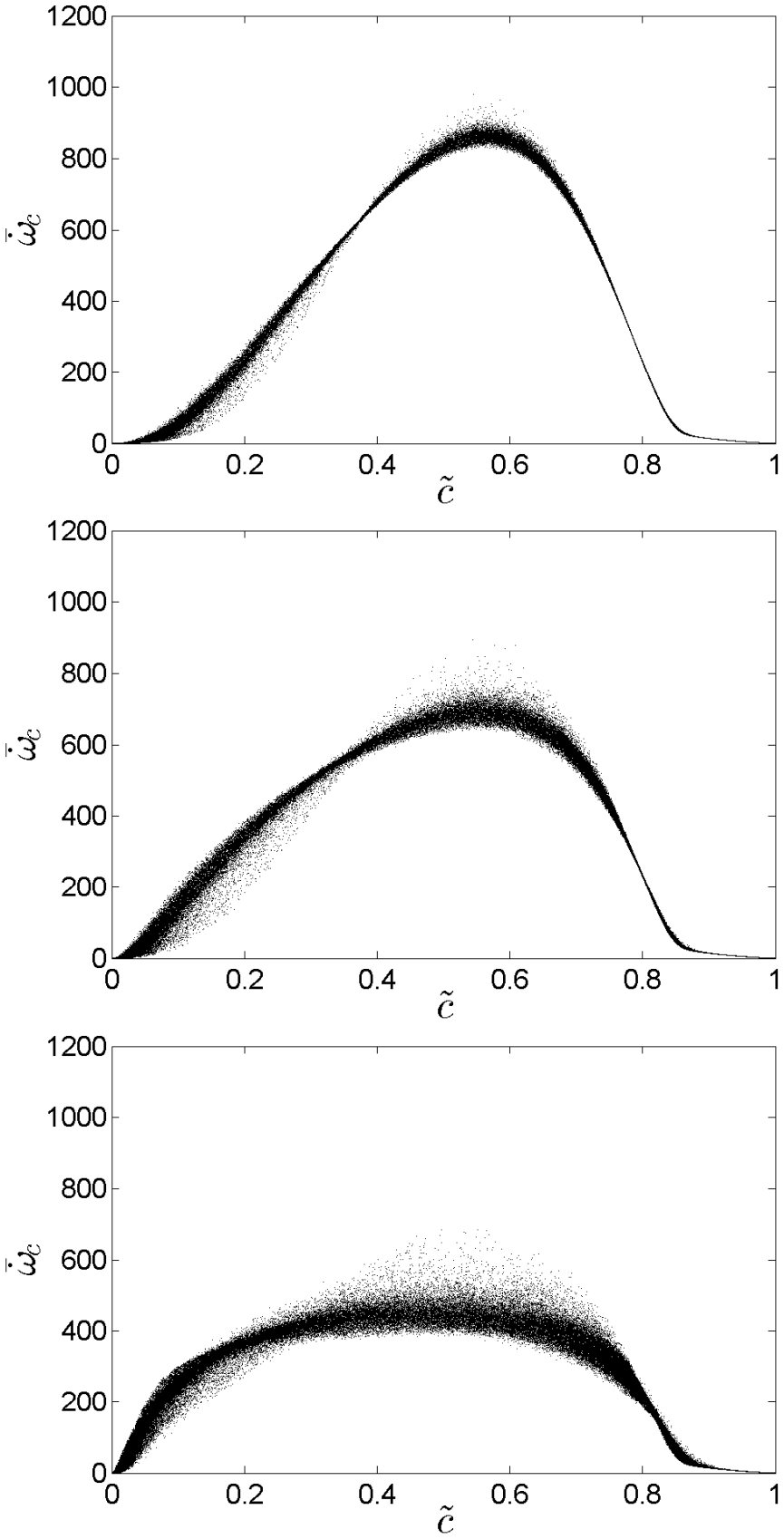

Figure 4: Scatter plots of filtered source term $\bar{\dot{\omega}}_c$ $[kg/m^3s]$ for an instantaneous DNS field spatially filtered with $\Delta = 2$, 4 and 8 times h_{DNS} (top to bottom).

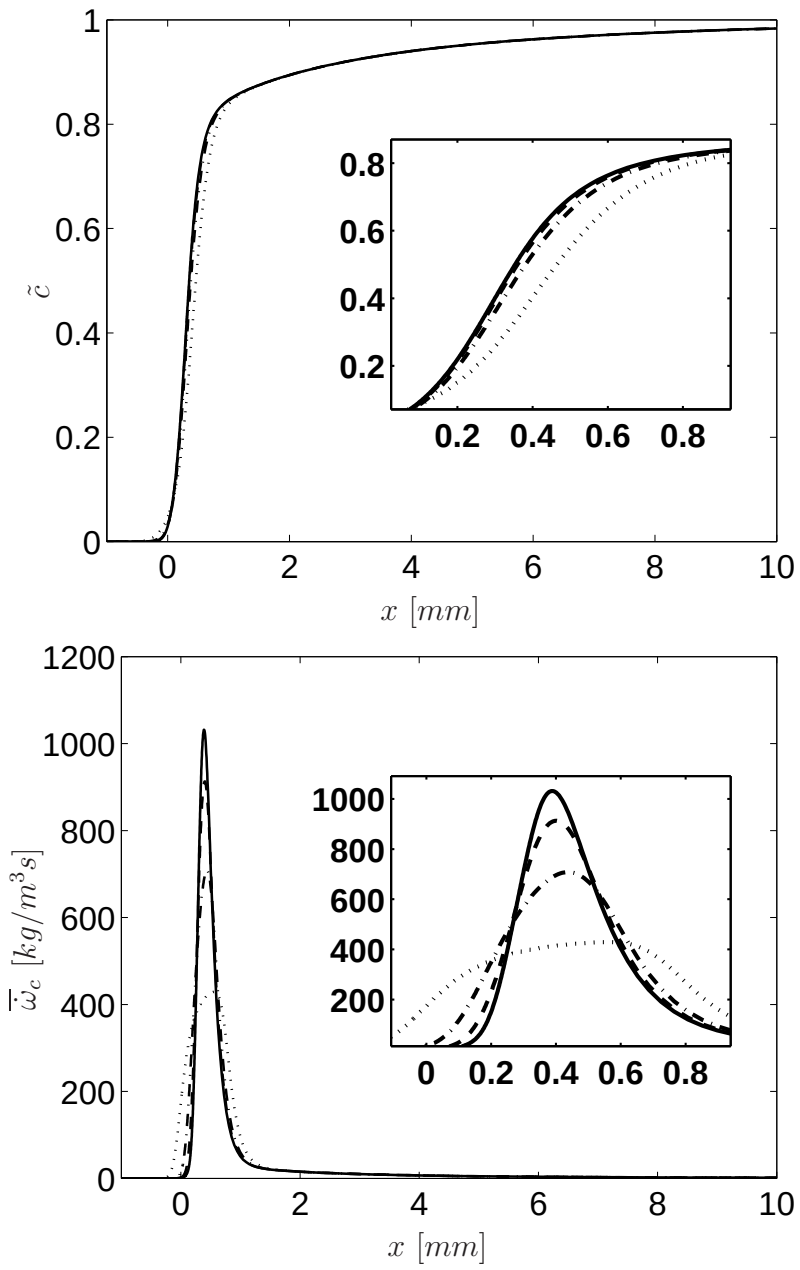

Figure 5: 1-D Flamelet convoluted in physical space with a top-hat of width 2 (dashed), 4 (dash dotted) and 8 (dotted) times h_{DNS}. The unfiltered laminar flame is shown by the solid line. The inset shows a zoom.

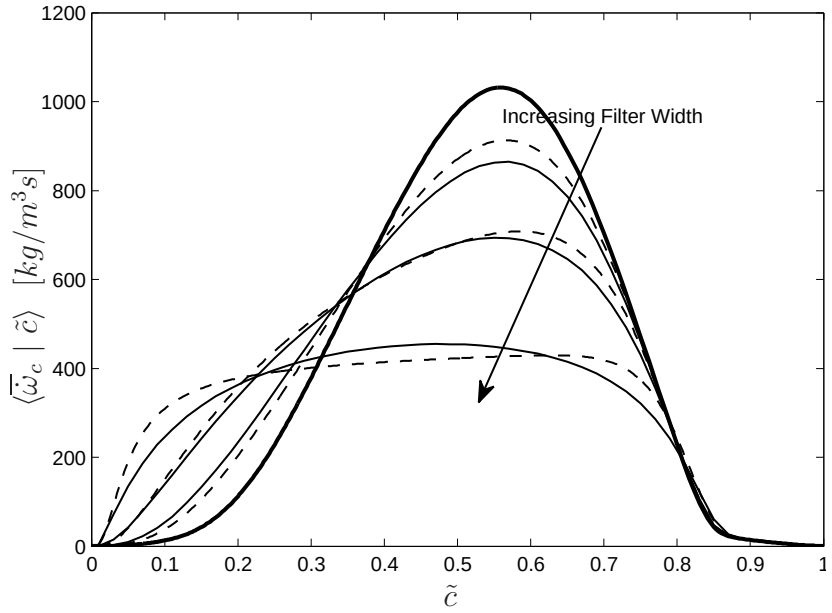

Figure 6: The filtered source term (thin solid lines) obtained by convoluting DNS data with a 3D top-hat filter of width $\Delta = 2$, 4 and 8 times h_{DNS} and the unfiltered source term (thick solid line) are shown in progress variable space. Filtered source terms obtained by convoluting a Flamelet with 1-D top-hat filter of identical filter widths i.e. $\Delta_f = \Delta$ are shown by dashed lines. For the DNS, data is first spatially filtered, then conditioned on $\tilde{c}$, and finally averaged in time.

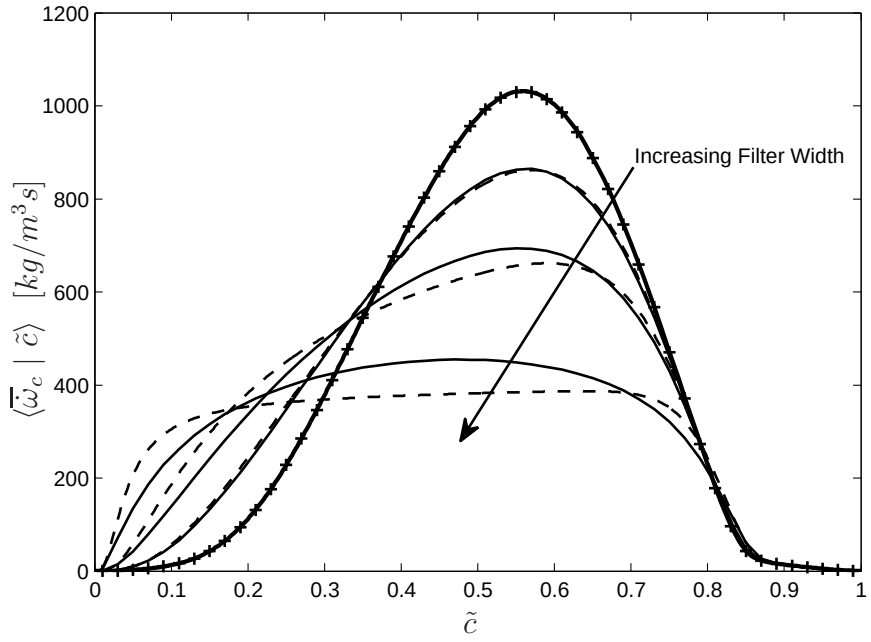

Figure 7: Source term for spatially filtered DNS (solid lines) at $\Delta = 2$, 4 and 8 times h_{DNS} and spatially filtered laminar flame (dashed lines) filtered at $\Delta_f^o = 2.5$, 4.5 and 9 times h_{DNS}. The unfiltered source term from DNS (line) and from 1-D laminar flame (symbols) coincide. For the DNS, data is first spatially filtered, then conditioned on $\tilde{c}$, and finally averaged in time.

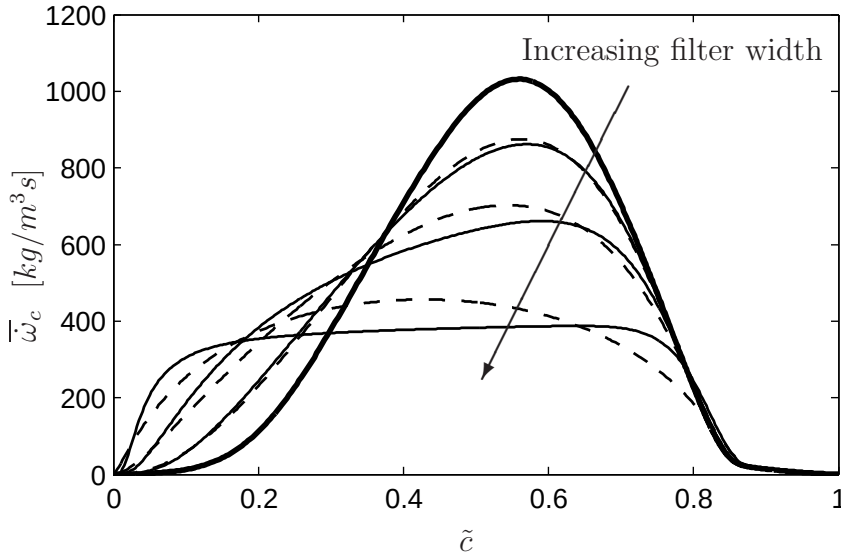

Figure 8: Filtered source term distribution against $\tilde{c}$ for Gaussian (dashed) and top-hat (solid) kernels of width (Δ_f^o) 2.5, 4.5 and 9 times h_{DNS}. Unfiltered source term is denoted by a thick solid line.

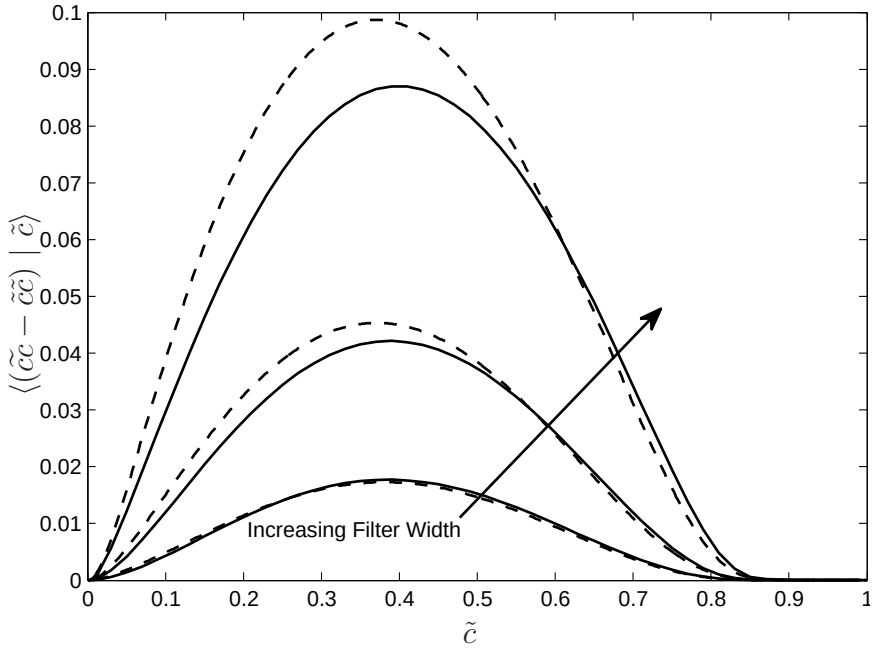

Figure 9: Progress variable variance c_v, for spatially filtered DNS(solid lines) at $\Delta = 2$, 4 and 8 times h_{DNS} and spatially filtered laminar flame(dashed lines) filtered at $\Delta_f^o = 2.5$, 4.5 and 9 times h_{DNS}. For the DNS, data is spatially filtered, then conditioned on $\tilde{c}$, and averaged in time.

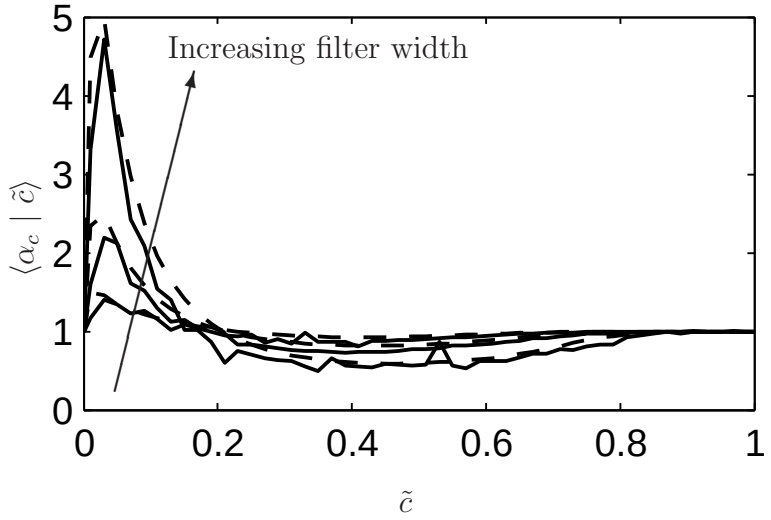

Figure 10: Diffusive correction factor (α_c) obtained by filtering streamwise diffusion term from DNS filtered at different Δ (solid lines) and from 1-D flame filtered at corresponding Δ_f^o (dashed lines).

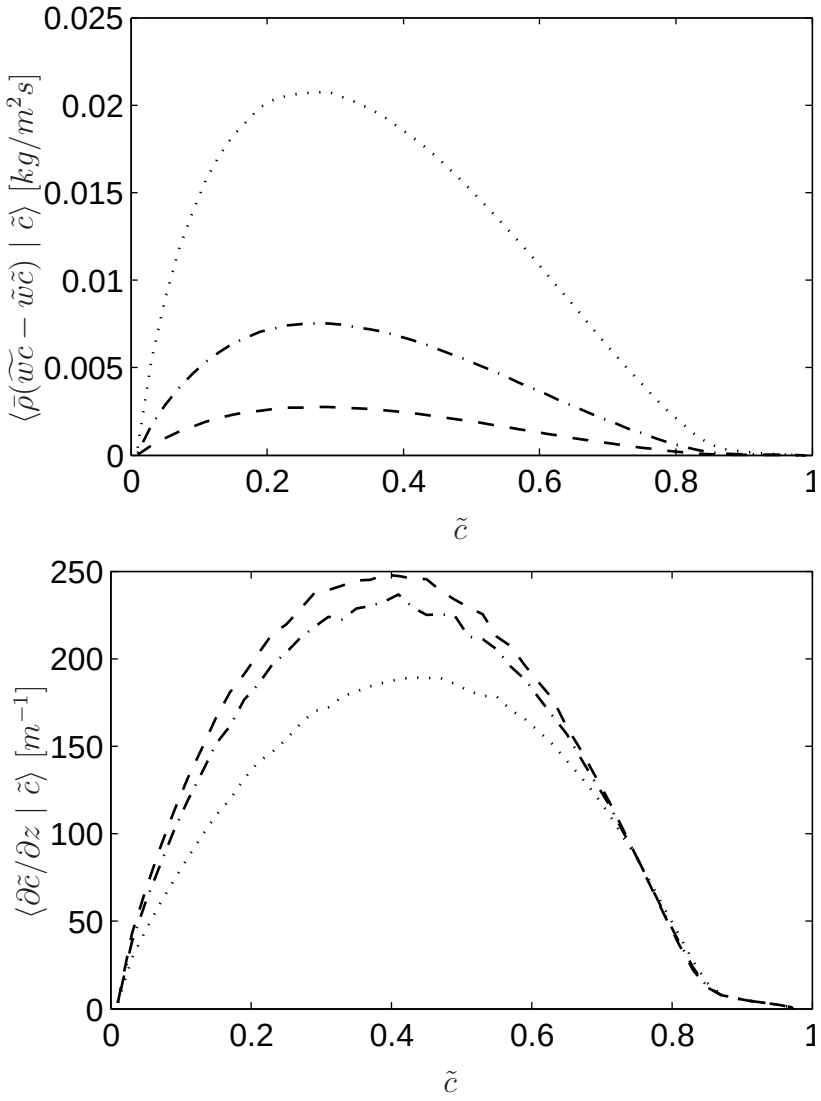

Figure 11: Unresolved flux of progress variable, $\bar{\rho}(\widetilde{wc} - \tilde{w}\tilde{c})$ (top), and gradient of progress variable, $\partial\tilde{c}/\partial z$ (bottom) in stream wise direction (z), computed from DNS filtered at $\Delta = 2$ (dashed), 4 (dash dotted) and 8 (dotted) times h_{DNS}.

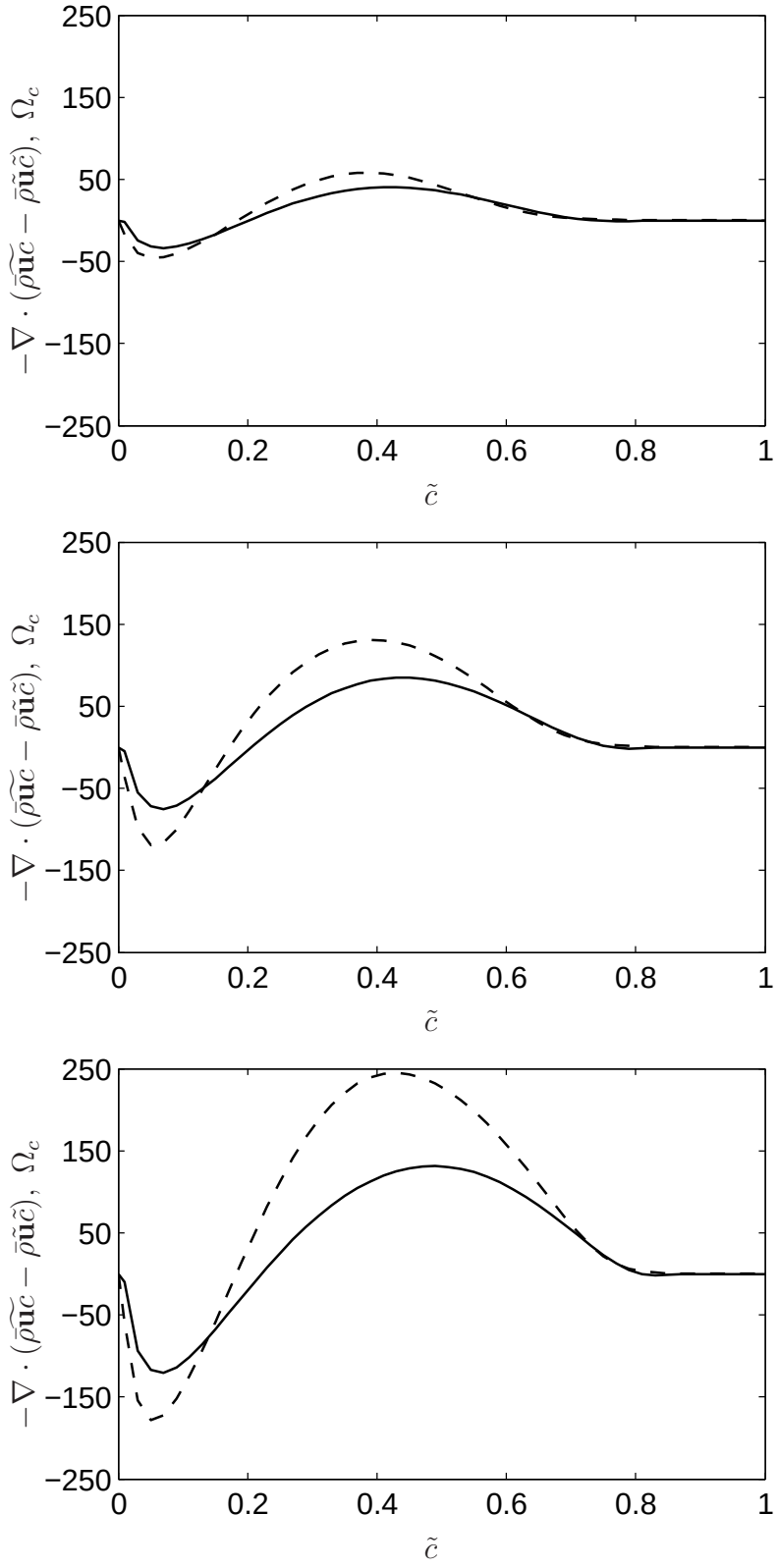

Figure 12: Unresolved or SGS scalar flux term $[kg/m^3s]$ computed from DNS, $-\nabla\cdot(\widetilde{\bar{\rho}\mathbf{u}c}-\bar{\rho}\tilde{\mathbf{u}}\tilde{c})$ (solid) filtered at $\Delta = 2$, 4 and 8 times h_{DNS} (top to bottom) and from 1-D flame, Ω_c (dashed) filtered at corresponding Δ_f^o .

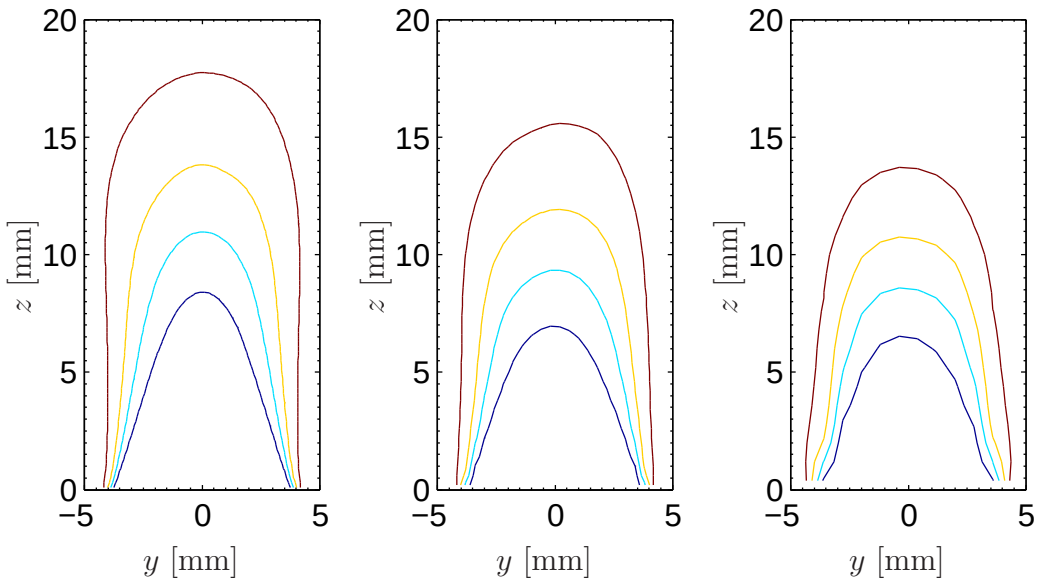

Figure 13: Averaged progress variable field from FFGM based on isocontours of $\tilde{c} = 0.2$, 0.4, 0.6 and 0.8 at a spatial resolution of (left to right) $h_x = 2$, 4 and 8 h_{DNS}.

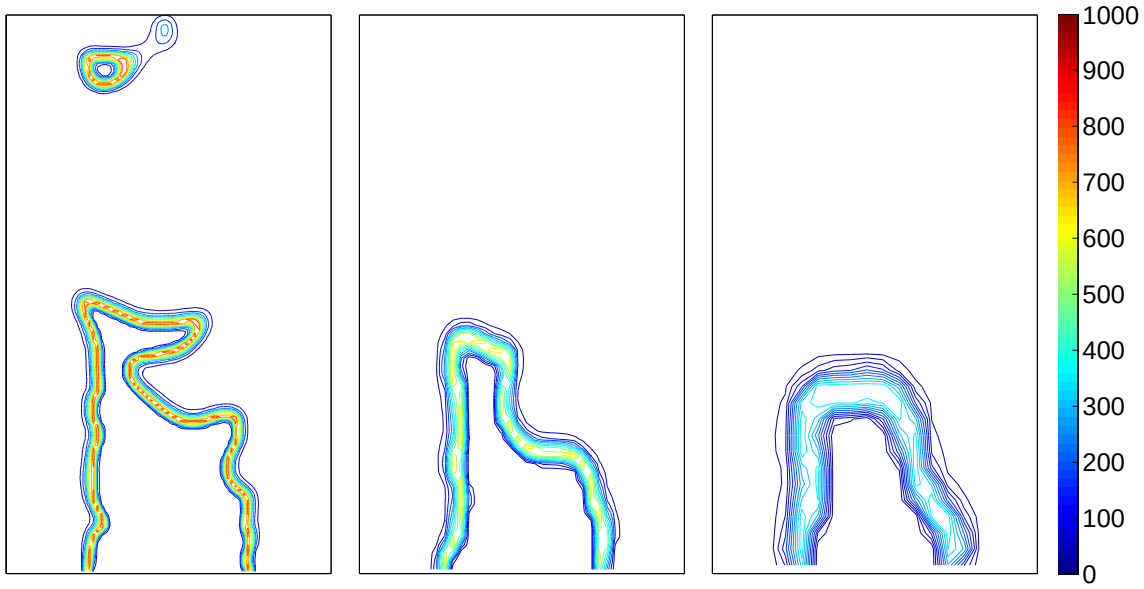

Figure 14: Instantaneous source term, $\bar{\dot{\omega}}_c$ $[kg/m^3 s]$ snapshots for FFGM at a spatial resolution of (left to right) $h_x = 2$, 4 and 8 h_{DNS}.

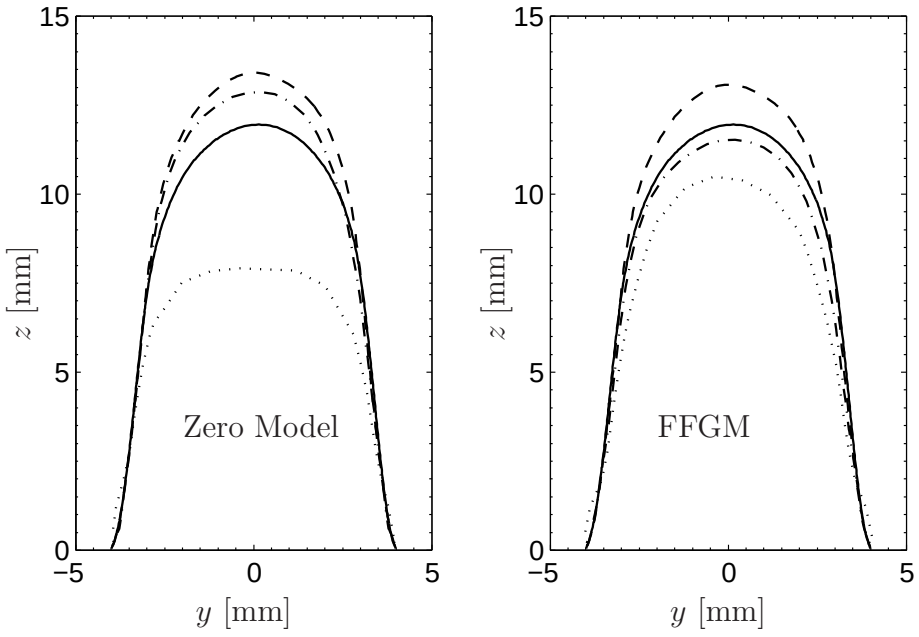

Figure 15: Flame shape represented by isocontour of $\tilde{c} = 0.55$ for zero model and FFGM model at $h_x = 2$ (dashed), 4 (dash dotted) and 8 (dotted) times h_{DNS}. The contour from DNS is represented by a solid line.

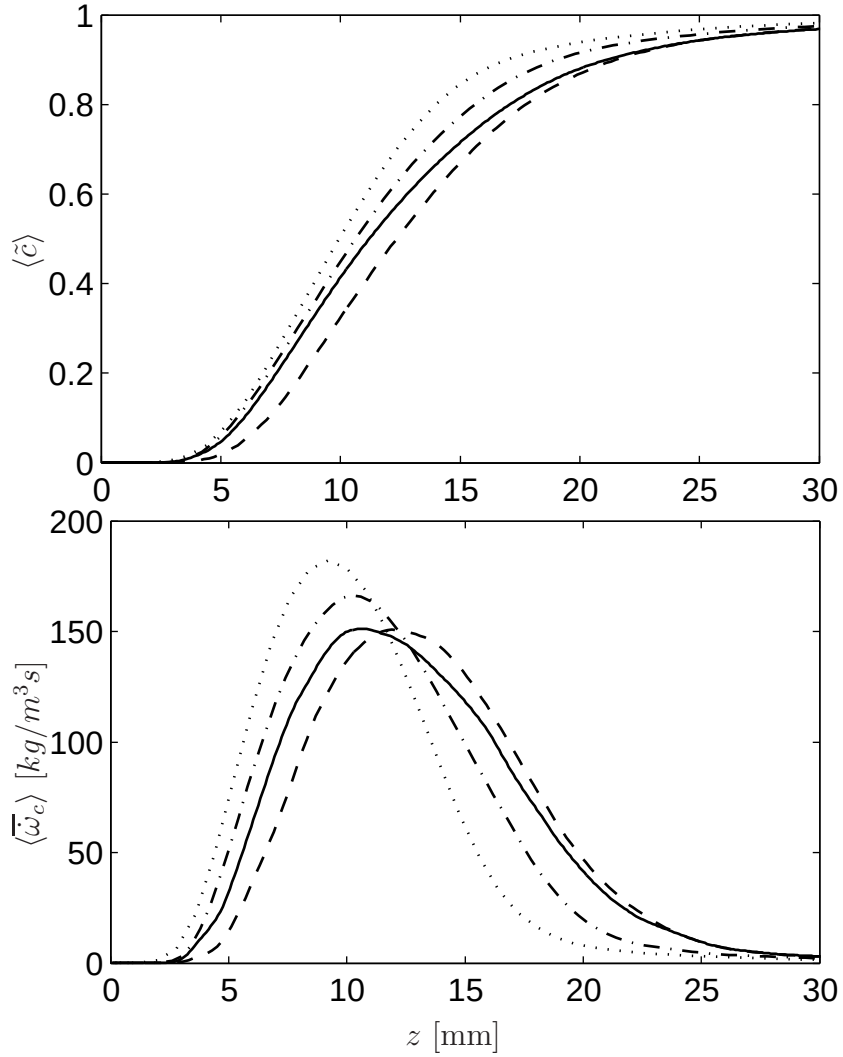

Figure 16: Centerline values of mean progress variable (top) and mean source term (bottom): DNS (solid) and FFGM at $h_x = 2$ (dashed), 4 (dash dotted) and 8 (dotted) times h_{DNS}.

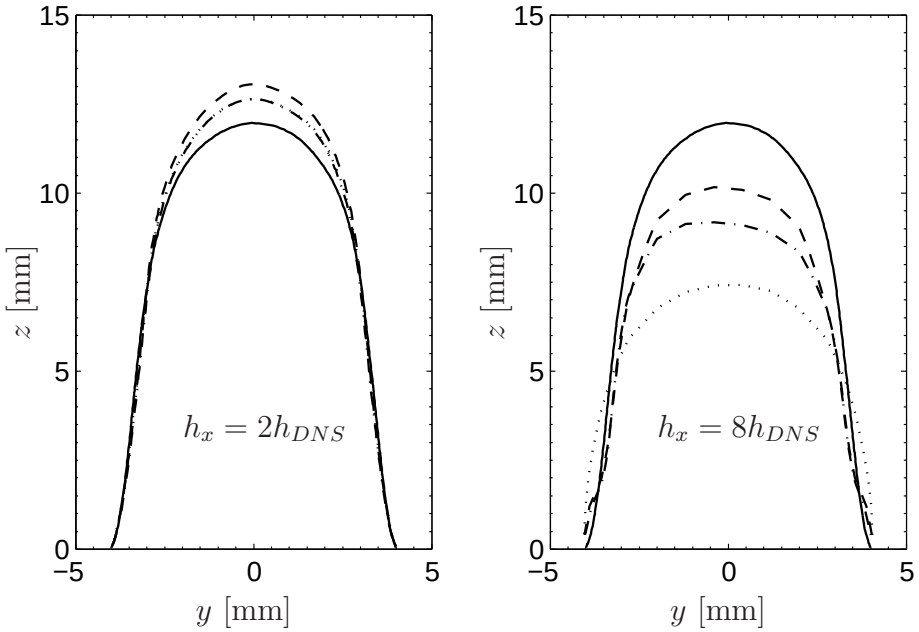

Figure 17: Effect of different closure terms on filtered progress variable equation is shown through prediction of flame shape denoted by isocontour of $c = 0.55$ for mesh size of $h_x = 2$ (left) and 8 (right) times h_{DNS} using flamelet filtered at corresponding Δ_f^o. The various closures compared are FFGM (dashed line), dropping diffusion correction from FFGM, i.e., $\alpha_c = 1$ (dash dotted) and dropping convective correction from FFGM, i.e., $\Omega_c = 0$ (dotted). In case of $h_x = 2h_{DNS}$ the curves with $\alpha_c = 1$ and $\Omega_c = 0$ overlap. The result from DNS is shown with solid line.

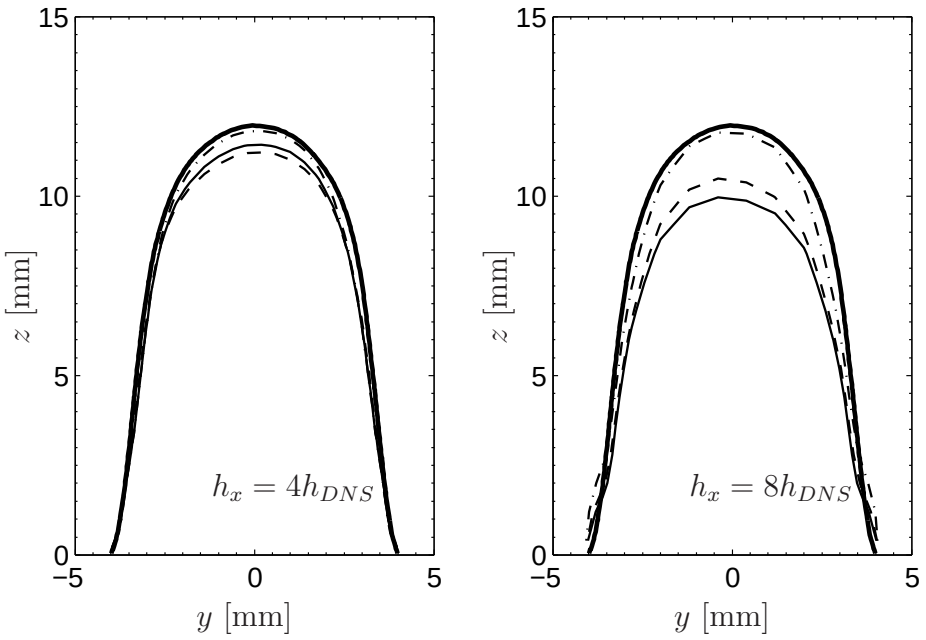

Figure 18: Effect of using manifold filtered at different widths on flame shape denoted by isocontour of $c = 0.55$. The manifolds are filtered at $\Delta_f = \Delta$ (dashed line), $\Delta_f = \Delta_f^o$ (solid) and $\Delta_f = \Delta_f^x$ (dash dotted). The flame shape from DNS is shown with a thick solid line.

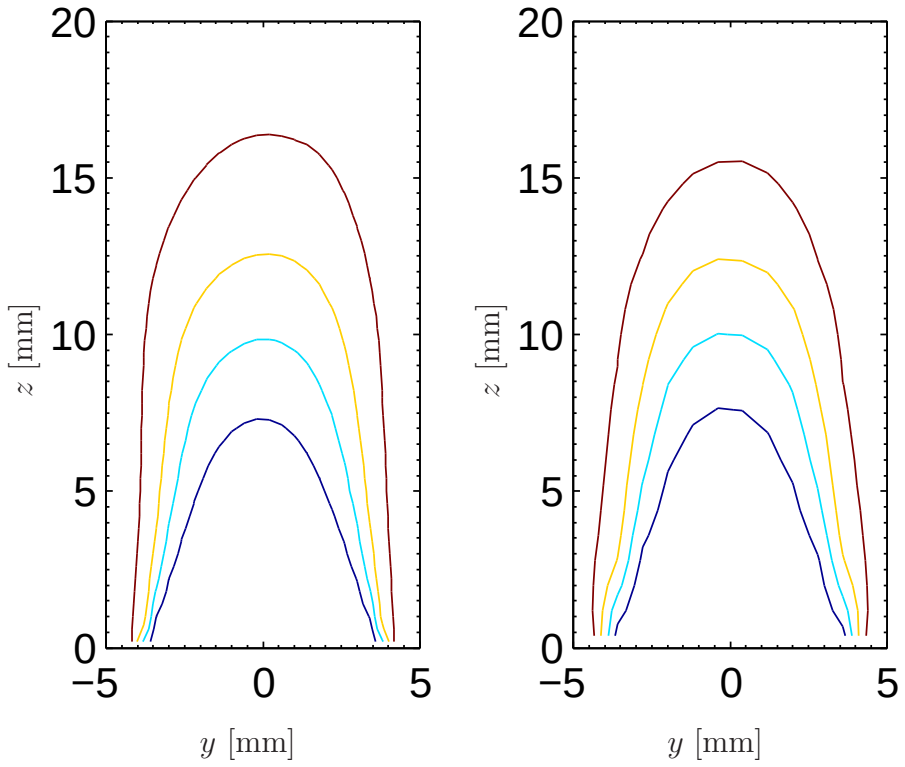

Figure 19: Averaged progress variable field based on isocontours of $\tilde{c} = 0.2$, 0.4, 0.6 and 0.8 at a resolution of $h_x = 4h_{DNS}$ (left) and $h_x = 8h_{DNS}$ (right) with FFGM using a flamelet filtered at corresponding Δ_f^x.

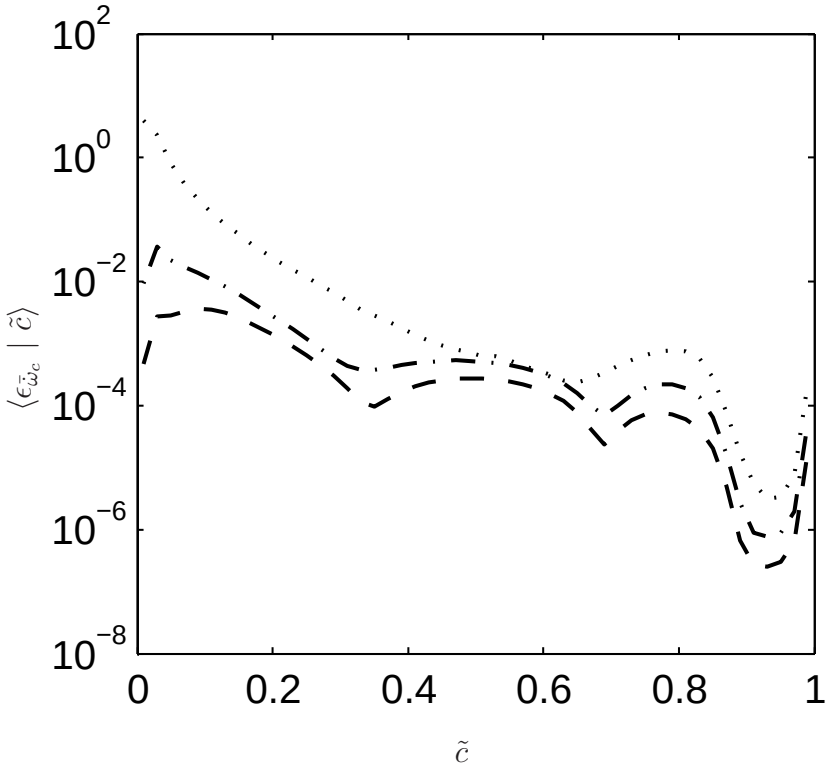

Figure 20: Semi-log plot of modeling error in $\overline{\dot{\omega}}_c$ filtered at 2 (dashed) , 4 (dash dotted) and 8 (dotted) times h_{DNS}, conditioned on $\tilde{c}$ and time averaged.